Optimized Automatic Fault Electrode Management of Structural Health Monitoring of Aircraft Composites

Ngoc Nam Pham, Jan Leuchter, and Erik Blasch, *Fellow, IEEE*

***Abstract*—Detecting the structural integrity of composite material used in an airframe includes passive nondestructive testing (NDT) and active electrical impendence tomography (EIT). EIT benefits enhance real-time response and accuracy but require pragmatic approaches to analyze the electrode errors from faulty or nonresponsive readings. The nonfunctional connections of measuring electrodes often occur during onboard aircraft operations for various reasons, such as deterioration. The deterioration of the electrode impedance impacts the quality of the EIT reconstructed image. This article compares different EIT methods and proposes surface fault detection EIT (SURFEIT). The proposed SURFEIT techniques that detect and compensate for faults are verified and evaluated using models with different locations of inside damages. Results prove the effectiveness of SURFEIT techniques, when the number of faulty electrodes is up to one-fourth of the total electrodes. The biggest benefit of the SURFEIT techniques is that they do not require any additional simulation work, lead to significant reduction of computation time, and afford very fast indications of damage locations.**

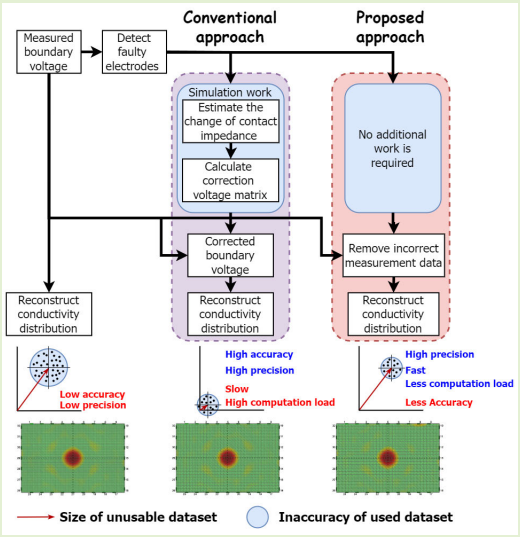

***Index Terms*— Data compensation, electrical impedance tomography (EIT), manage faulty electrodes.**

I. Introduction

THE use of composite materials has expanded in the last decades from bikes and boats to autonomous cars and electronic aircraft. Composites, along with metals, plastics, and ceramics, are the four main types of engineering materials. In contrast to other types of materials, composites are the combinations of at least two distinct materials (constituents), different at the molecular level and mechanically separable. At the macroscopic level, although the constituents retain their original form, as well as chemical, mechanical, and physical properties, material combinations create better properties for the composite. Compared with traditional engineering materials, composites provide diverse advantages, such as lightweight, high specific stiffness and strength, and high resistance against corrosion. Moreover, composites offer the ability to fabricate complex geometry parts without welding or riveting. Notably, composites allow "modulation" of properties, for example, modulation of thermal expansion coefficient to the values of zero, by adjusting the ratio of constituents. These advantages make composites preferred materials as compared to conventional materials in various applications. Particularly, composites are popular in load-bearing structures in special applications, such as aerospace, transportation, and wind turbines [1], [2], [3], [4], [5], [6].

On the other hand, the practical use of composites can encounter numerous limitations, such as sensitivity to moisture and temperature, low temperature and electrical conduction, and risk of galvanic corrosion with aluminum. Aluminum is one of the most common engineering metals for aircraft due to its lightweight. Furthermore, there is a major obstacle

Received 8 August 2024; revised 9 September 2024; accepted 9 September 2024. Date of publication 18 September 2024; date of current version 31 October 2024. This work was supported in part by the Modern Micro- and Nano-Electronics for Futures under Project FEKT-S-23-8162 and in part by the Brno University of Technology. The associate editor coordinating the review of this article and approving it for publication was Dr. Chinthaka Gooneratne. *(Corresponding author: Jan Leuchter.)*

Ngoc Nam Pham is with the Faculty of Electrical Engineering and Communication, Department of Microelectronics, Brno University of Technology, Brno 61600, Czech Republic (e-mail: 243756@vutbr.cz).

Jan Leuchter is with the Faculty of Electrical Engineering and Communication, Department of Microelectronics, Brno University of Technology, Brno 61600, Czech Republic, and also with the Faculty of Transport Engineering, Department of Electrical and Electronic Engineering and Signalling in Transport, University of Pardubice, Pardubice 53210, Czech Republic (e-mail: leuchter@upce.cz).

Erik Blasch is with MOVEJ Analytics, Dayton, OH 45324 USA (e-mail: erik.blasch@gmail.com).

Digital Object Identifier 10.1109/JSEN.2024.3459614

in detecting and evaluating damages or defects in composite structures to maintain structural integrity whether actively or passively. The mechanical properties and service life of composite structures can be significantly affected by damage accumulated in the composite structure. Although a small delamination in composite structure may not immediately cause dangerous issues, it can lead to hazardous risks affecting the operational safety of the structure [1], [2], [3], [4], [5], [6], [7], [8]. The use of multiple sensors can enhance safety concerns by analyzing the redundancy and determining the faulty sensors [9], [10].

To address concerns about detecting and evaluating damage or defects in composite materials, nondestructive testing (NDT) methods have been an essential possibility. NDT can be defined as a discipline including evaluation and inspection processing of a structure to detect or characterize damage or defect without altering the original characteristic or harming the structure under test. Therefore, NDT offers the ability to detect indiscernible damage inside the composite structure to increase operational reliability and safety of the structure, as well as minimize the maintenance expense. There are numerous NDT methods applied at different stages of a composite structures' lifespan. The most common NDT methods for composites include visual inspection, acoustic emission, ultrasonic testing, and electromagnetic testing techniques [6], [11], [12], [13], [14], [15].

In recent years, structure health monitoring (SHM) has been proposed as a potentially useful enhancement to NDT. The benefit of SHM is that it extends the ability of NDT to continuously, real-time monitoring of composite structures and detects the existence and initiation of damage. Conventional SHM approaches use external sensors for the purpose of monitoring the structure. Other types of sensors, such as fiber-optic sensors, piezoelectric sensors, or strain gauges, have been embedded to composite structure. Combined with the data-driven sensing, the modeling of the structure with finite-element model (FEM) approaches offers increased dynamic real-time response [16].

However, the approach of embedding sensors to composite structures might cause unwanted effect to the properties of the structures. Therefore, the approach to use electrical impedance tomography (EIT) has been referred to as a promising complement to NDT. EIT is not a new technique, and it is widely considered to have originated in 1978, as documented in [17]. Initially, the EIT development primarily targeted medical applications. Subsequently, the use of the EIT method has been applied to geophysics and industrial process monitoring. Due to numerous advantages, including inexpensive, noninvasive, and high temporal resolution, EIT has recently been presented as an additional SHM technique [18], [19], [20], [21], [22], [23].

This article deals with one of the most significant issues occurring in the practical implementation of EIT-based SHM systems, which is the impact of faulty electrodes (poorly connected or detached electrodes) on the generated tomography image. The faulty sensor reading might cause a noticeable quality decrease of the regenerated tomography image and hence negatively affect the effectiveness of EIT-based SHM

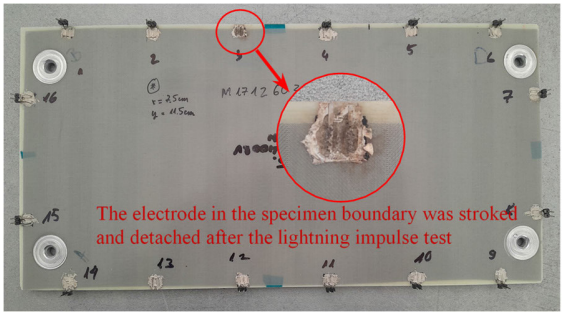

Fig. 1. Composite specimen under lightning impulse test. An electrode in the specimen boundary was stroked and detached after the test.

systems to detect damage. The issue is that when one or more electrodes are detached or in the case of parallel EIT acquisition systems proposed in [24], one or more analog-to-digital converters (ADCs) are damaged during operation. As an example, for EIT systems implemented in aircraft, a lightning strike to aircraft might cause the detachment of some electrodes or damage some ADCs. Another example is shown in Fig. 1, which shows a composite specimen under a lightning impulse test. One of the electrodes prepared in the boundary of specimen for EIT measurement was struck with energy and detached after the test. The result is the existence of unreliable measurements data in the dataset.

This article proposes novel surface fault detection EIT (SURFEIT) method to automatically detect the faulty electrodes and modify the model, as well as dataset of boundary voltage based on the detection of faulty electrodes. The advantages of the proposed SURFEIT method can be listed as better automatic detection of faulty electrodes and less complexity in compensating the faulty measurement data due to reduced computation procedures during preprocessing. Less complex computation allows minimizing total time, computational load, and hardware requirements of EIT-based SHM systems. As discussed in the following, less complex computation also helps to eliminate the impact of computation errors on the reconstructed images. It is important to emphasize that computation error is not neglectable in practical digital computational systems. The novel proposed method in this article is compared to the methods proposed in [25] and [26] to verify their effectivity.

II. Electrical Impedance Tomography

The basis task of EIT is to reconstruct the conductivity distribution of the object under test (OUT). The problems in EIT are divided into two categories—the forward and inverse problem. The forward problem calculates the boundary voltage distribution based on the known injection current and conductivity distribution, while the inverse problem tries to estimate the conductivity distribution from the known boundary voltage distribution. This article presents the basis of EIT technique, including the mathematical model and measuring or calculating the principles of forward and inverse problems.

A. Forward Problem—Well-Posed Problem

The function of EIT forward problem is to solve the object's information given known initial parameters. The EIT forward

problem is to determine the voltage distribution in OUT, while the conductivity distribution of the object and injection current is known. Such a problem is considered as a well-posed problem, because of its existence, uniqueness, and stability. The first way to solve the EIT forward problem is through the direct measurement of a physical object. The electrodes are placed around the boundaries of the OUT. Through these electrodes, a current is injected into the OUT, and the boundary voltage is measured. There are several measurement strategies, such as adjacent drive method, opposite method, cross method, or the trigonometric method developed for EIT forward problems [27], [28]. This article uses adjacent drive, also called as the neighboring method. Injection current I is applied to a neighboring electrode pair, while the boundary voltage is measured between the remaining electrode pairs.

Another way to solve EIT forward problems is using numerical methods. The EIT forward problem can be mathematically presented using Maxwell's equations and Ohm's law, with the assumption that the OUT does not have any internal current source and using quasi-static electric field expression [25], [26], [27], [28], [29], [30]

$$\begin{cases} \boldsymbol{J} = \sigma \boldsymbol{E} & (1) \\ \nabla \cdot \boldsymbol{J} = 0 & (2) \\ \boldsymbol{E} = -\nabla \varphi & (3) \end{cases}$$

where $\boldsymbol{J}$ is the current density, $\boldsymbol{E}$ is the electrical field, σ is the conductivity distribution, and φ is electrical potential. Solving (1)–(3), we obtain the equation describing the relationship between conductivity distribution and voltage distribution of OUT as

$$\nabla \cdot (\sigma \nabla \varphi) = 0. \tag{4}$$

There are different techniques to solve the EIT forward problem, among which finite element method (FEM) is the most preferred way. The OUT is meshed into several discrete elements from the FEM component models. With the assumption of small conductivity perturbation, the variation of boundary voltage against conductivity change can be approximated as [25], [26], [27], [28], [29], [30]

$$\Delta U = J \Delta \sigma \tag{5}$$

where ΔU is the change of boundary voltage, $\Delta \sigma$ is the conductivity perturbation, and J is the Jacobian matrix.

B. Inverse Problem—Ill-Posed Problem

The inverse problem is the process that calculates the object's information based on measurement results. The EIT inverse problem calculates the conductivity distribution of OUT based on the boundary voltage values and injection current. The Jacobian matrix described in (5) is also the basis for the calculation of conductivity distribution. In opposite to the forward problems, the inverse problem is known as an ill-posed problem, where a minor perturbation in the boundary voltage values can cause significant errors in calculated conductivity distribution. In addition, the total boundary voltage values are much smaller than the required pixels in the regenerated tomography, and hence, different conductivity distributions might produce the same boundary voltage values.

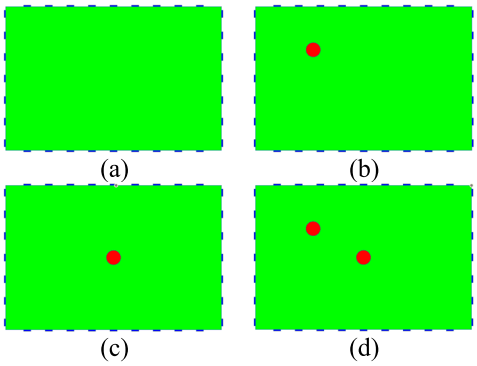

Fig. 2. Model under simulation in this article. (a) Without damage and (b)–(d) first, second, and third cases of damage location.

The EIT inverse problem can be categorized into absolute and differential imaging. While the absolute imaging technique tries to reconstruct conductivity distribution inside OUT, the differential imaging technique refers to reconstructing the changes in conductivity distribution between different states of OUT [29], [31], [32]. The absolute imaging technique can be formulated by (6) and the differential imaging technique can be formulated by (7)

$$\hat{\sigma} = \arg\min\left(\|J\sigma - U\|_2^2\right) \tag{6}$$

$$\hat{\Delta\sigma} = \arg\min\left(\|J\Delta\sigma - \Delta U\|_2^2\right). \tag{7}$$

It was concluded that differential imaging generally offers more stable reconstruction of conductivity distribution [29], [31], [32]. This article focuses on detecting and localizing the defect on the OUT. Therefore, the differential imaging method called Gauss–Newton one-step is used to calculate the change in conductivity distribution of OUT. Current studies conclude that a high-quality reconstructed image can be obtained by using Newton's one-step error reconstruction (NOSER) algorithm. However, accurate conductivity values are not guaranteed [29], [33], [34]. For the task of detection and localization damage on the OUT, the conductivity values are less important than the quality of reconstructed image.

In this article, forward problem is solved in simulation. The inverse problem is solved using the Electrical Impedance and Diffuse Optical Tomography Reconstruction Software (EIDORS) [35] using the NOSER algorithm. The composite specimen shown in Fig. 1 is modeled by a rectangle model with 32 electrodes located around specimen boundary at different intervals. The simulation was conducted with three cases of damage location inside the model, as shown in Fig. 2.

III. Proposed Technique

This article proposes a novel surface fault EIT method to detect and eliminate the effects of a frequently encountered problem in EIT systems: detached or poorly connected electrodes. Such issues originate significant errors in the measurement data, leading to inaccurate reconstructed tomography results and affecting the ability to detect and localize damages in the OUT. Several studies present methods to eliminate these effects, with a common approach illustrated in Fig. 3 [25], [26], [30], [36], [37].

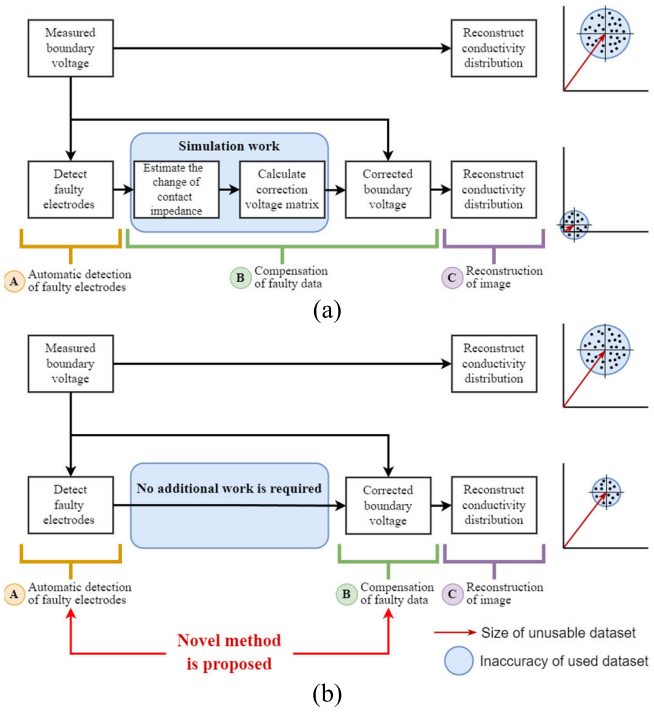

Fig. 3. Approach to compensate the effect of faulty electrodes. (a) Conventional approach and (b) proposed approach.

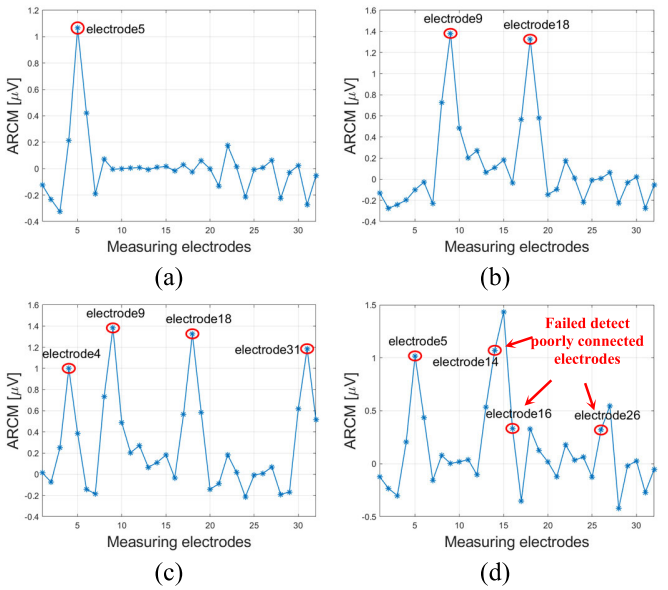

Fig. 4. Verification of using ARCM-based techniques in rectangle model with electrodes placed at different intervals and with different numbers of poorly connected electrodes. The order of poorly connected electrodes is randomly selected. Poorly connected electrodes are shown. (a) One electrode is poorly connected. (b) Two electrodes are poorly connected. (c) and (d) Four electrodes are poorly connected.

In first process (process A), faulty electrodes are (automatically) detected based on the analysis of measured boundary voltage. Currently, the presented methods proposed several analyses to detect faulty electrodes. This article proposed our SURFEIT analyses based on analyzing the ratio of standard derivation (RSD) of measured boundary voltage. The results presented in next part prove that the proposed method eliminates drawbacks of other methods.

In the second process (process B), conventional methods use FEM simulation work to estimate the change in contact impedance at faulty electrodes, where these estimated values are employed to calculate the correction voltage matrix. The measured boundary voltages are corrected using this matrix before being used to reconstruct the conductivity distribution. The compensation effectively eliminates the effects of electrode peeling, allowing for accurate calculation of the conductivity distribution from the full set of boundary voltage values.

However, the conventional methods have a limitation: the steps of estimating the contact impedance change and calculating the compensation voltage matrix require FEM simulations, which demands knowledge of the material properties of the OUT and a sufficiently accurate model for precise calculations. Additionally, because the necessary values, such as contact impedance changes or correction voltage matrices, are estimated by interpolation or extrapolation, sufficient simulation datasets are required, resulting in significant time consumption and computational workload when processing data.

This article proposes a novel method to automatically detect faulty electrodes and to compensate faulty data in measurement dataset without additional FEM simulation. The proposed SURFEIT method offers a solution with high efficiency, minimum time consumption, and hardware requirements.

A. Automatic Detection of Faulty Electrodes

There are several techniques published to detect the faulty electrodes (detached or poorly connected electrodes) based on the analysis of measured voltage values. As an instance, in [25], the poorly connected electrodes are detected by analyzing the average relative change of measurement voltage (ARCM) calculated for each measuring electrode by

$$\mathrm{ARCM}_k = \frac{1}{2(N-4)} \sum_{i=1}^{2(N-4)} \left| U'_{i_k} - U_{i_k} \right| \tag{8}$$

where k is the order of measuring electrode, N is the total number of measuring electrodes, $2(N-4)$ is the total number of boundary voltage values measured at concerned (kth) electrode, and U'_{i_k} and U_{i_k} are the ith boundary voltage measured at concerned (kth) electrode with poorly and well-connected electrodes. This technique was verified using circular model with electrodes placed around the boundary at equal intervals and an opposite current driving mode [25].

Our task, however, uses a rectangular model with electrodes placed around boundary at different intervals and adjacent current driving mode. The verification of ARCM-based technique in our task with random selection of poorly connected electrodes is shown in Fig. 4. Note that in an EIT system with an adjacent current driving mode, the total number of boundary voltage measured at concerned electrode is $2(N-3)$, but not $2(N-4)$, as in the case of opposite current driving mode. The results show that the ARCM-based technique can detect faulty electrodes at almost cases. However, in the cases when the kth and $(k+2)$th electrodes are faulty, the ARCM-based techniques cannot be applied, and the ARCM_{k+1} is indicated as a local maximum, but not ARCM_k nor ARCM_{k+2}. The reason is that boundary voltages measured at $(i+1)$th electrode are under the effect of both ith and $(i+2)$th electrodes.

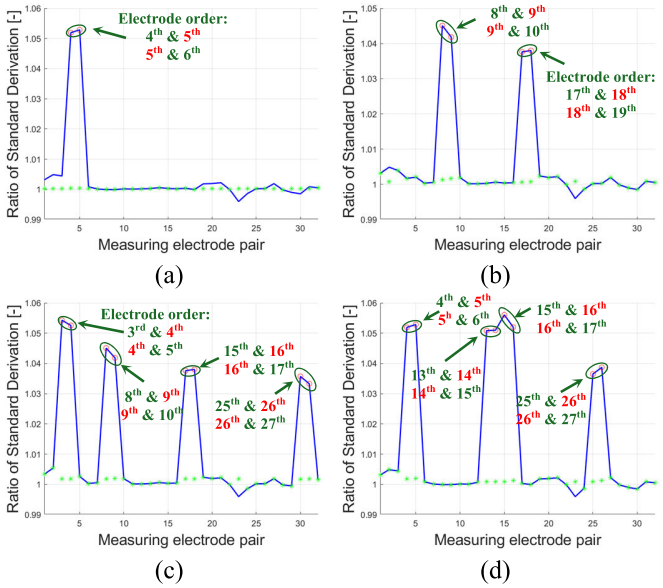

Fig. 5. Verification of using the proposed techniques in rectangle model with electrodes placed at different intervals and with different numbers of poorly connected electrodes. The order of poorly connected electrodes is randomly selected. Poorly connected electrodes are marked in red. (a) One electrode is poorly connected. (b) Two electrodes are poorly connected. (c) and (d) Four electrodes are poorly connected.

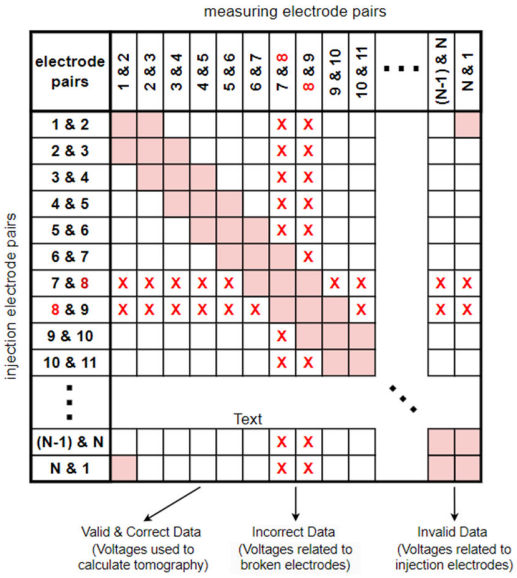

Fig. 6. Illustration of the SURFEIT method for the case of an N-electrodes EIT system, in which electrode number 8 is detached or poorly connected, making the data measured at this electrode is incorrect.

This article, therefore, proposes a novel approach and technique to detect the detached or poorly connected electrode that can detect these problem electrodes in any case. The proposed SURFEIT approach does not focus on detecting faulty electrodes; however, it detects the electrode pairs boundary voltages measurements, which are affected by the change of contact impedance. The proposed techniques are based on RSD, which is calculated by

$$\mathrm{RSD}_n = \frac{\sigma'_n}{\sigma_n} = \frac{\sqrt{\frac{\sum_{l=1}^{N-3}\left(U'_{n_l}-\overline{U'_n}\right)}{N-3}}}{\sqrt{\frac{\sum_{l=1}^{N-3}\left(U_{n_l}-\overline{U_n}\right)}{N-3}}} \tag{9}$$

where n is the order of concerned electrode pair, N is the total number of measured electrode pairs, $N-3$ is the total number of boundary voltage measured at concerned (nth) electrode pair, σ'_n and σ_n are the standard deviations of boundary voltages measured at the nth electrode pair with poorly and well-connected electrodes, and U'_{n_l} and U_{n_l} are the lth boundary voltage measured at concerned (nth) electrode with poorly and well-connected electrodes.

From experiments, SURFEIT is able to conclude that due to the impact of contact impedance changes, the RSD value calculated at the measuring electrode pairs affected by poorly connected electrodes will be much higher than the RSD value calculated at the remaining electrode pairs. In our work, the RSD values are processed by Hampel filter to detect the outliers, which indicate affected measuring electrode pairs. The proposed SURFEIT technique is verified in the same cases as to be used to verify the ARCM-based technique. Verification results are shown in Fig. 5, which shows that the proposed SUREFIT techniques have eliminated the weakness of the ARCM-based technique presented above.

B. Compensation of Faulty Measurement Dataset

The effect of faulty electrodes in adjacent current driving mode is illustrated in Fig. 6. It is common to present measured data by a matrix, in which the row number indicates the number of injection electrode pairs and the column number indicates the number of measuring electrode pairs. Since the voltage measured at injection electrode is typically unused to eliminate the significant effect of contact impedance, these data in the matrix are signed as invalid data (by red color). In this illustrated case, with the assumption that electrode number 8 is detached, or poorly connected, hence, the measurement data related to electrode 8 are referred to incorrect data. Using matrix representation, it obviously indicates the incorrect data measured at electrode number 8 and the entire data measured when electrode number 8 is injected.

As mentioned above, most of the techniques presented to compensate for inaccurate data in current studies require extensive simulation work with the knowledge of material properties and can be highly time-consuming. The advantage of these simulation techniques is the high precision of the compensated dataset, resulting in highly accurate reconstructed tomography and conductivity values, allowing better determination of the shape and size of the heterogeneous region. Our research, however, focuses on fast detection and localization of damage inside OUT. The conductivity values are less important than total computation time. Therefore, the proposed SUFEIT technique discards the incorrect data, instead of trying to correct them before calculating the conductivity distribution.

The SURFEIT technique results in the need to modify the EIT model due to the removal of incorrect data. It is not simply a matter of removing electrode 8 from the EIT model, because the measured voltage between electrodes 7 and 9, nor the measured voltage when current flows between these electrodes, is available. More precisely, the predetermined measurement

strategy of the EIT model needs to be revised. Correction is performed in two independent steps. The first is that the injection strategy is adjusted to eliminate injections associated with faulty electrodes; and the second is to eliminate the boundary voltage measured at the faulty electrodes.

To verify the proposed technique, the models described in Fig. 2 were used. The simulated scenario is that the contact impedance at electrode number 8 is increased. The boundary voltage is then processed using the SURFEIT technique and technique introduced in [25], where the correction of boundary voltage is calculated based on the estimated value of contact impedance variation η. To estimate the η value, the mean relative change (MRC) of boundary voltage is defined as

$$\mathrm{MRC} = \left| \frac{1}{N(N-4)} \sum_{i=1}^{N-4} \sum_{k=1}^{N} \left(U'_{i_k} - U_{i_k} \right) \right| \tag{10}$$

where k is the order of measuring electrode, N is the total number of measuring electrodes, $N(N-4)$ is the total number of boundary voltage values, and U'_{i_k} and U_{i_k} are the ith boundary voltage measured at concerned (kth) electrode with poorly and well-connected electrodes [25].

It is also important to emphasize that the MRC-based technique was developed for absolute imaging, where the EIT inverse problem is more sensitive to variations of the contact impedance. The MRC-based technique, therefore, was developed with the change of contact impedance up to 250%. In the case of differential imaging in this article, such a small change does not cause serious effect in reconstructed image. In this article, the MRC-based technique is verified with significant increase of the contact impedance, up to nearly infinity (when electrodes are detached). The different interested region of contact impedance changes results in the different regression relationship between MRC and η. As shown in Fig. 7, the dependence of η on MRC in our study cannot be approximated as linear. The reasons for nonlinear relationship can be the difference of model shape (circular versus rectangle), the distribution of electrodes in specimen boundary, or the distance between electrodes. In our study, the distribution of electrodes cannot be freely selected. The applied object of our developed SHM system is aircraft composite structure. The goal is to avoid using additional electrodes on these structures so as not to affect their structural and mechanical properties, and hence, rivets for installing these structures are used as electrodes. As a result, for each composite structure, in which our developed SHM system is applied, a simulation dataset with corresponding regression function is required that makes a further barrier to correct the faulty data by simulation work.

In this article, the relationship between MRC and η is referred to two-term exponential approximation, which is formulated as

$$\mathrm{MRC} = \alpha \times e^{\gamma \times \eta} + \beta \times e^{\delta \times \eta} \tag{11}$$

where $\alpha = 0.084$, $\beta = -0.085$, $\gamma = 0.002$, and $\delta = 0.014$. Using (11), one is able to estimate the contact impedance of faulty electrodes and then calculate the correction matrix for boundary voltage. The tomography is then reconstructed using

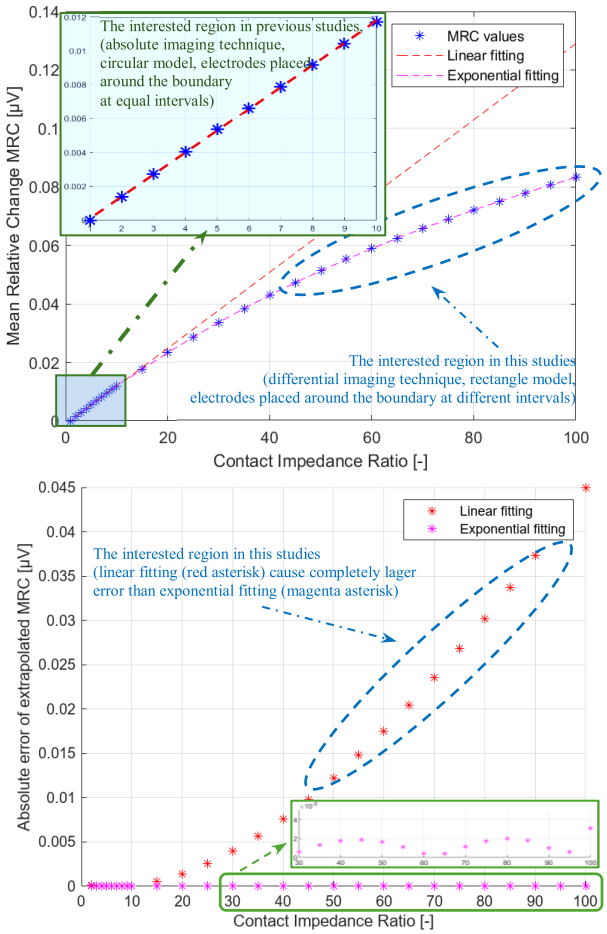

Fig. 7. Increase of accuracy by using more suitable fitting function. The exponential fitting offers smaller error.

Model number	Reference model	1% error in parameter calculation	2% error in parameter calculation	5% error in parameter calculation
1st				
2nd				
3rd				

Fig. 8. Effects of error in parameter calculation in reconstructed images.

boundary voltage values corrected by using the methods shown in Fig. 3.

The values of parameters α, β, γ, and δ in (11) play an important role in the accuracy of solution. Any inaccuracies in the calculation of these parameters impact the estimated value of the contact impedance of faulty electrodes, which in turn affects the values of the correction matrix for boundary voltage. For instance, Fig. 8 illustrates the reconstructed images when the parameters of the fitting function in (11) are computed with errors of 1%, 2%, and 5%. The results

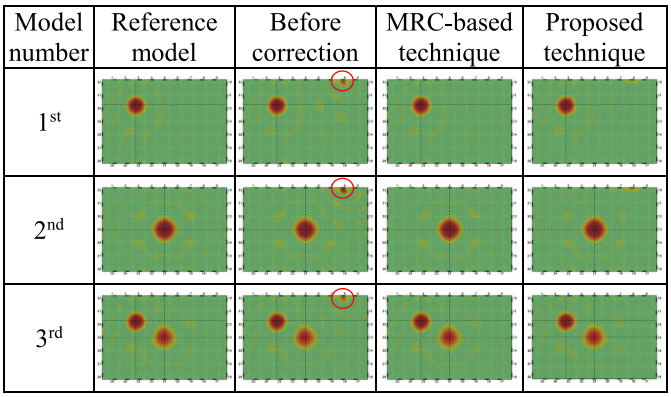

Fig. 9. Verification of the proposed technique to eliminate the faulty data.

indicate that even minor changes in the values of the fitting function's parameters can significantly reduce the effectiveness of data correction. This issue is a notable drawback of current methods. The SURFEIT method aims to correct the boundary voltage dataset without relying on the extrapolation process, thereby reducing computation errors, which are significant in practical computation systems.

To verify the proposed SURFEIT technique, the forward problems of rectangle models with different damage levels are shown in Fig. 2 and solved in simulation. The results of forward problems are then used to reconstruct the tomography of these models. The reconstructed tomography using MRC-based technique and the SURFEIT technique is shown in Fig. 9.

From Fig. 9, it can be observed that the SURFEIT technique has comparable effectiveness to MRC-based technique in compensating the faulty data. The artifacts caused by detached or poorly connected electrodes are successfully removed. The tomography clearly shows the location of damages inside the OUT. When combined with the technique for automatically detecting faulty electrodes, SURFEIT can swiftly identify and compensate for the effects of these faulty electrodes. SURFEIT does not require any additional simulations, which reduces the overall processing time and computational load, enabling rapid detection of damage within OUT. However, SURFEIT does not encourage accurate conductivity values, which are necessary for diagnosing the size and severity of the damage. More detail evaluations of SURFEIT are presented in the next part.

IV. Results and Evaluation

The proposed SURFEIT technique is compared with other techniques presented in previous studies. Fig. 3 illustrates the SURFEIT procedure for eliminating the effects of damaged electrodes. The procedure includes two phases, where in the first phase (A), the measured data are analyzed in order to detect damaged electrodes. Based on the detection, the accuracy of the measured data can be analyzed, and then, the measured data that are less accurate can be removed. With this procedure, it is possible to refine the resulting measured data in order to improve the quality of the "reconstructed image."

In the second phase (B), a model of OUT is assembled, which includes information about the distribution of electrodes

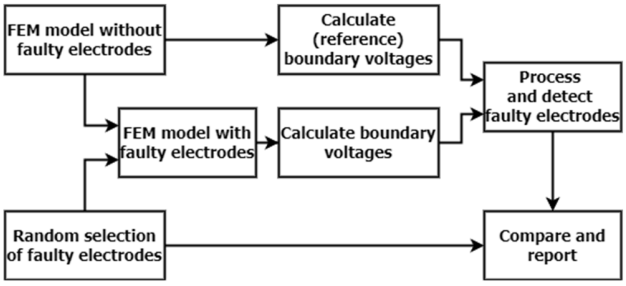

Fig. 10. Test bench to statically evaluate the proposed technique to detect detached or poorly connected electrodes.

TABLE I
Evaluation Effectiveness of the Proposed Technique

Number of poorly connected or detached electrodes	Number of test cases	Electrodes are poorly connected		Electrodes are detached	
		Number of correct detections	Ratio of correct detections	Number of correct detections	Ratio of correct detections
1	32	32	100 %	32	100 %
2	50	50	100 %	50	100 %
3	50	50	100 %	50	100 %
4	50	50	100 %	50	100 %
6	50	50	100 %	50	100 %
8	50	50	100 %	50	100 %
10	50	33	66 %	44	88 %

on the sample and the order of measurements. Then, the model is modified based on the selected electrodes (measured data) from the previous phase (A). This improves the fit between the built model and the selected measured data. In this way, an increase in the overall performance of "image reconstruction" can be achieved. SURFEIT improves the overall display of the conductivity distribution of the sample and, therefore, it is also possible to obtain better results of detection and localization of defects in the composite test sample.

The SURFEIT technique detects and compensates for faulty electrodes as successfully verified in selected cases. It is clear from the results that it is not possible to verify all possible combinations; therefore, we made a selection based on the principles of static methods for a better automated evaluation.

A. Automatic Detection of Faulty Electrodes

To evaluate SURFEIT, an emulator test bench is designed to statically evaluate its ability to detect faulty electrodes, as shown in Fig. 10. The test bench randomly selects electrodes, which are referred as to detached or poorly connected. The boundary voltage values calculated by FEM are analyzed by SURFEIT to automatically detect the affected measuring electrode pairs. The detection is then compared with the selected faulty electrodes under simulation to verify the results, as shown in Table I. SURFEIT has been shown to detect faulty electrodes with high accuracy. It can correctly identify all affected measuring electrode pairs when up to eight electrodes (or one-fourth of the total electrodes number) are poorly connected or detached.

The proposed SURFEIT technique is also compared with the techniques presented in [36] and [37] (see Fig. 11).

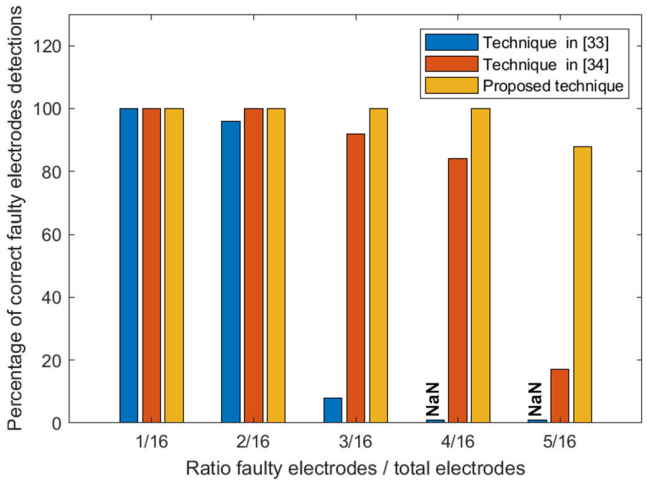

Fig. 11. Comparison of the proposed technique to detect faulty electrodes with other technique presented in [36] and [37].

These techniques are compared in terms of accurate detections of all faulty electrodes. It can be concluded from Fig. 11 that SURFEIT provides better performance. With the increase in the number of faulty electrodes up to one-fourth of the total electrodes number, SURFEIT can accurately detect all defective electrodes, while other techniques can only detect some of them.

B. Compensation of Faulty Data

The proposed SURFEIT that compensates for faulty measurement data caused by poorly connected or detached is also evaluated using similar method as to evaluate the proposed technique to automatically detect faulty electrodes. One or more random selected electrodes in the model are referred to as poorly connected and detached. The number of faulty electrodes is chosen as 1, 2, 4, 7, and 8. The boundary voltage data are calculated using FEM. The inverse problem is then solved using faulty data and using data compensated by SURFEIT. To compare, the voltage-replacement method (VRM) and voltage-shift method (VSM) techniques presented in [26] are also used to solve inverse problem. These techniques are selected because they also compensate for faulty dataset without additional simulation work. As discussed above, our study avoids the need for additional simulation work to adapt with the applications, where the detail information about material is not available, and the time need to detect damage inside OUT is more important.

The metrics, such as relative root mean square error (RRMSE) and structural similarity index measure (SSIM), are calculated for quantitative evaluation and comparison of mentioned techniques. The formulations for calculation of RRMSE and SSIM are

$$\text{RRMSE} = \frac{\|\sigma - \sigma_0\|}{\|\sigma_0\|} \tag{12}$$

$$\text{SSIM} = \frac{(2 \cdot \bar{\sigma} \cdot \bar{\sigma_0} + C_1)(2 \cdot \text{cov}(\bar{\sigma}, \bar{\sigma_0}) + C_2)}{(\bar{\sigma}^2 + \bar{\sigma_0}^2 + C_1)(\text{var}(\bar{\sigma}) + \text{var}(\bar{\sigma_0}) + C_2)} \tag{13}$$

where σ and σ_0 denote the conductivity distributions of reconstructed tomography and original ones (in this case, the reference model); C_1 and C_2 are constants to avoid division by zero. The RRMSE is required to be as small as possible, while the SSIM is required to be closest to 1 to achieve accurately reconstructed images. The poorly reconstructed images have RRMSE value much higher than 1 and SSIM values much smaller than 1.

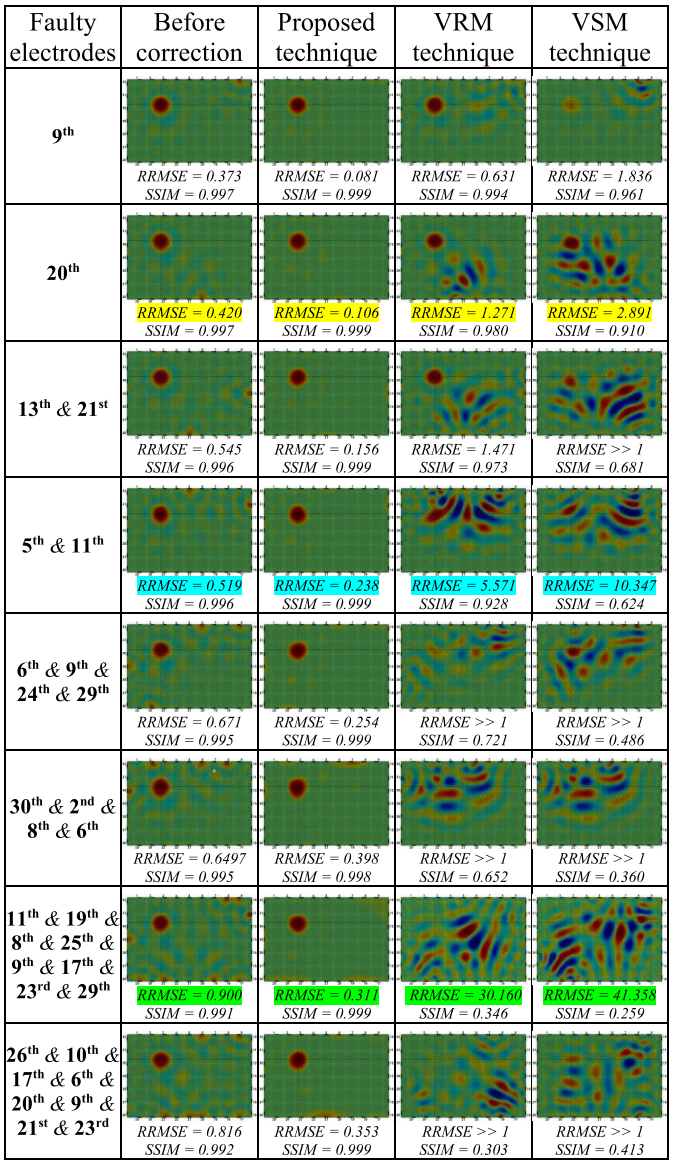

Fig. 12. Verification of the proposed method using the model number 1st, and electrodes are poor connected.

First, the proposed techniques are evaluated using model number 1 (see Figs. 2 and 9). The evaluation is shown above, where Fig. 12 shows the results when the contact impedance of selected electrodes is increased (the selected electrodes are poorly connected), and Fig. 13 shows the results when the selected electrodes are detached (their contact impedances have infinite values).

By visual comparison, the results demonstrate the value of the SURFEIT technique. In the case when faulty electrodes are poorly contacted, the VSM and VRM techniques can compensate for the faulty data when only one electrode is referred as faulty. With a higher number of faulty electrodes, VRM and VSM cannot provide reconstructed image with high quality to clearly detect the damage inside OUT.

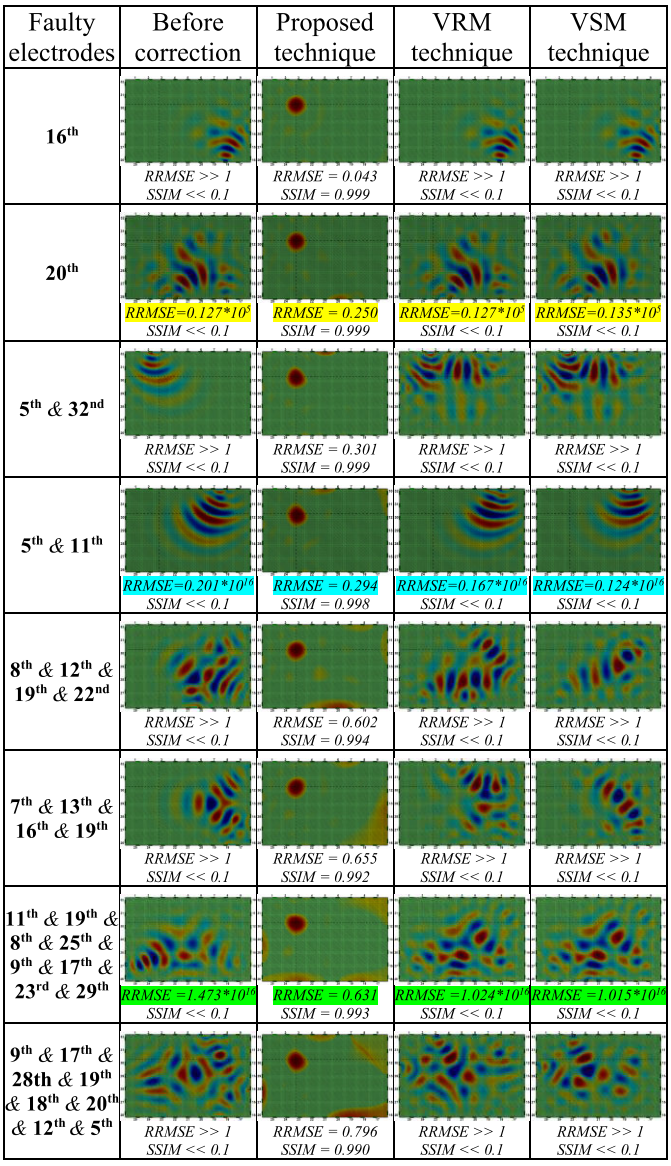

Fig. 13. Verification of the proposed method using the model number 1st, and electrodes are detached.

The quality of reconstructed images with VSM and VRM techniques is even lower than the reconstructed images without compensation. In comparison, the SURFEIT technique provides the ability to clearly detect damage inside OUT when the number of faulty electrodes is up to 8 (or one-fourth of total electrode numbers). In the second case, when faulty electrodes are detached, SURFEIT also provides reconstructed images, which clearly show the location of the damage inside OUT, while the reconstructed images using faulty data without compensation or using data corrected by other techniques do not indicate the location of damage inside OUT.

RRMSE and SSIM values also demonstrate similar conclusions. For example, Fig. 12 shows the case when electrode 20th is poorly connected to specimen (marked in yellow). The VRM and VSM techniques provide reconstructed image with low quality, shown by RRMSE values 1.271 and 2.891. As mentioned above, the RRMSE values are required to be as low as possible; the ideal values, even, are zero. In comparison, the proposed techniques can improve the quality of reconstructed images, with RRMSE value of 0.106, which is about four times smaller than the RRMSE value of reconstructed image before correction.

The similar case, when 20th electrode is disconnected, is shown in Fig. 13, also marked in yellow. In such a case, reconstructed images before correction and after correction using VRM and VSM techniques have RRMSE value in the order of 10^5, which are very poor values. Our proposed SURFEIT technique, again, provides a much better image, with the RRMSE value of 0.250. The RRMSE value in this case is about two times worse than the case when the 20th electrode is poorly connected.

Fig. 12 also presents the comparison when more electrodes are poorly connected and detached. In the case two electrodes (5th and 11th) are poorly connected (marked in cyan color), the proposed technique successfully compensates the faulty data and improves the RRMSE values from 0.519 (before correction) to 0.238, which is obviously better than 5.571(VRM technique) and 10.347 (VSM) technique. When eight electrodes (11th, 19th, 8th, 25th, 9th, 17th, 23rd, and 29th) are poorly connected (marked in green color), the proposed technique also improves the RRMSE values, from 0.900 (before correction) to 0.311, which is obviously better than 30.160 (VRM technique) and 41.358 (VSM) technique. If these electrodes are detached (marked in cyan and blue in Fig. 13), the RRMSE values of images with the proposed techniques are 0.294 and 0.631, when images before correction and images compensated by VRM and VSM techniques have RRMSE values in the order of 10^{16}.

Similar conclusion can be drawn for SSIM index. It can be seen from Fig. 12 that, in the cases when faulty electrodes are referred as poorly connected, the SSIM values of images reconstructed from faulty data (before correction) range from 0.991 to 0.997. After applying the proposed technique to compensate the faulty data, the SSIM index can achieve higher values, ranging from 0.998 to 0.999. The VRM and VSM techniques, however, do not conduct improvement the image quality, while they do significant decrease in SSIM values. The images with VRM techniques have SSIM in the range of 0.303–0.994, and the images with VSM techniques have SSIM values from 0.259 to 0.961.

In the case when faulty electrodes are detached (see Fig. 13), the SSIM values of images with data before correction and images with data compensated by VRM and VSM techniques have very low SSIM values, nearly zero. In comparison, the proposed SURFEIT technique offers reconstructed images with much higher SSIM, ranging from 0.990 to 0.999. Obviously, similar as RRMSE values, the SSIM values in the case of detached electrodes are also worse than in the case poorly connected electrodes, due to the large change in contact impedance of faulty electrodes.

The effectiveness of the SURFEIT technique to model number 2nd, see Fig. 9, is also evaluated. The reason for choosing these models is to verify and evaluate the proposed techniques for damage in different locations inside the OUT. Model number 1 contains 1 damage in the corner, while model number 2 has damage in the center of OUT. Fig. 14 shows the cases when faulty electrodes are poorly connected,

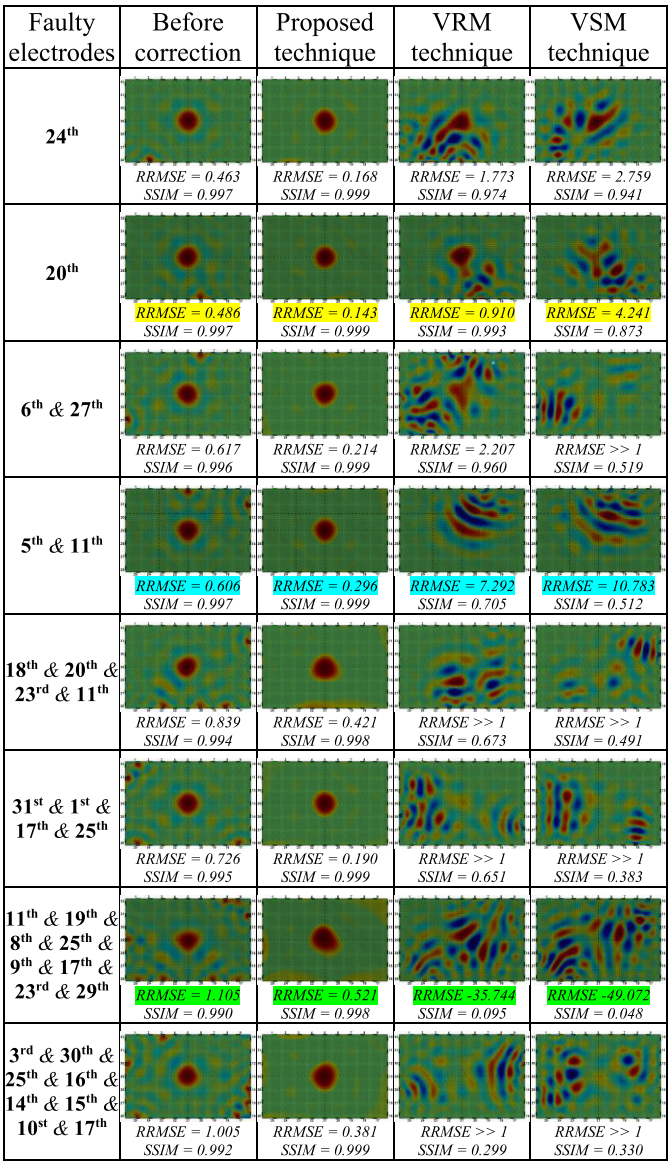

Fig. 14. Verification of the proposed method using the model number 2nd, and electrodes are poor connected.

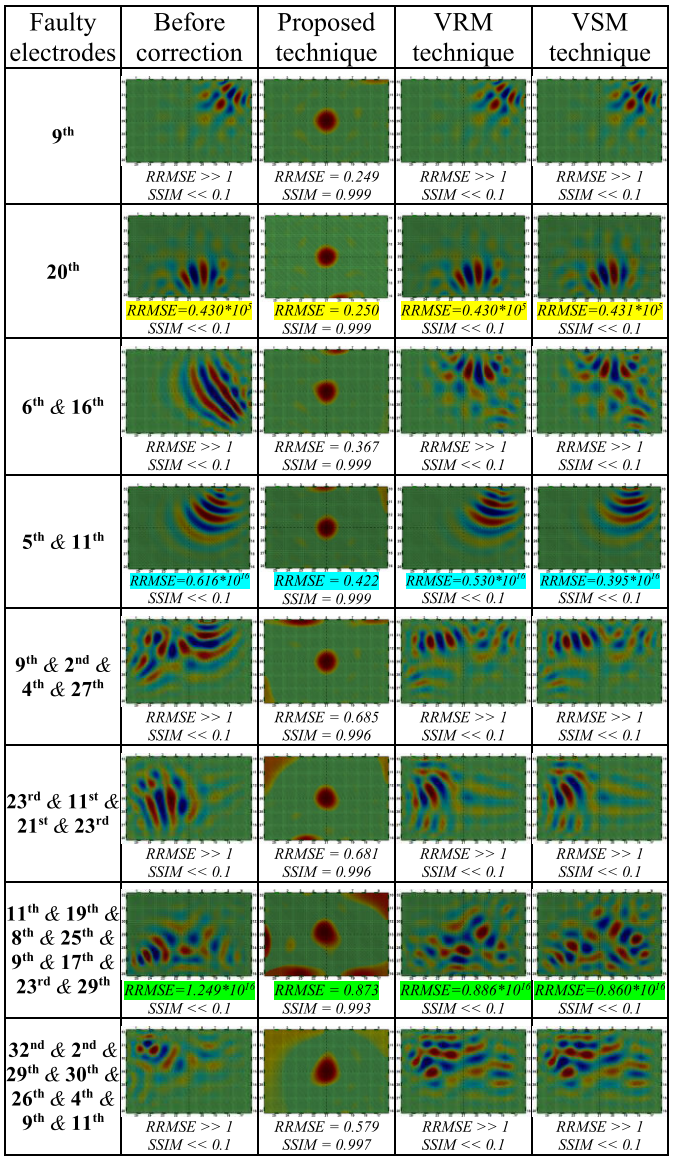

Fig. 15. Verification of the proposed method using the model number 2nd, and electrodes are detached.

and Fig. 15 shows the case when faulty electrodes are detached. Faulty electrodes in all cases are selected randomly.

Similar to model 1, the visual analysis can clearly demonstrate that, in all cases when faulty electrodes are poorly connected, the proposed techniques can remove the artifacts in the reconstructed images and offer better values of SSIM and RRMSE index. In the case when the faulty electrodes are detached, reconstructed images without compensation, or those compensated using VRM and VSM techniques, fail to clearly indicate internal damages. However, the reconstructed images using the proposed techniques can accurately pinpoint the locations of the damages.

The three cases analyzed above (number of faulty electrodes are 1, 2, and 8) are also tested in the 2nd model. When one electrode (the 20th electrode) is faulty, the RRMSE value is improved from 0.486 to 0.143 (in case of poorly connected electrode) and from the order of 10^5 to 0.250 (in case of detached electrode). In these two cases, the SSIM values increase to 0999 from 0997 and nearly zero, respectively. When two electrodes (the 5th and 11th electrodes) are faulty, the proposed technique offers RRMSE values of 0.296 and 0.422 and SSIM values of 0.999. In the next case, eight electrodes (the 11th, 19th, 8th, 25th, 9th, 17th, 23rd, and 29th electrodes) are poorly connected and detached, the RRMSE values within the proposed techniques are 0.521 and 0.873, and the SSIM values are 0.998 and 0.993. In all the case, it can be concluded that the proposed technique significantly improved the values of RRMSE and SSIM index, or in other words, the proposed techniques provide good compensation of faulty data and allow improving the quality of reconstructed image and the ability to correctly detect damage inside the OUT.

It can also be concluded that the damage in the center of the OUT is more sensitive to faulty electrodes than damage near the boundary of OUT. From the results shown in Figs. 12–15, it is clearly that when the faulty electrodes are identical in all of the cases, the values RRMSE index when the damage

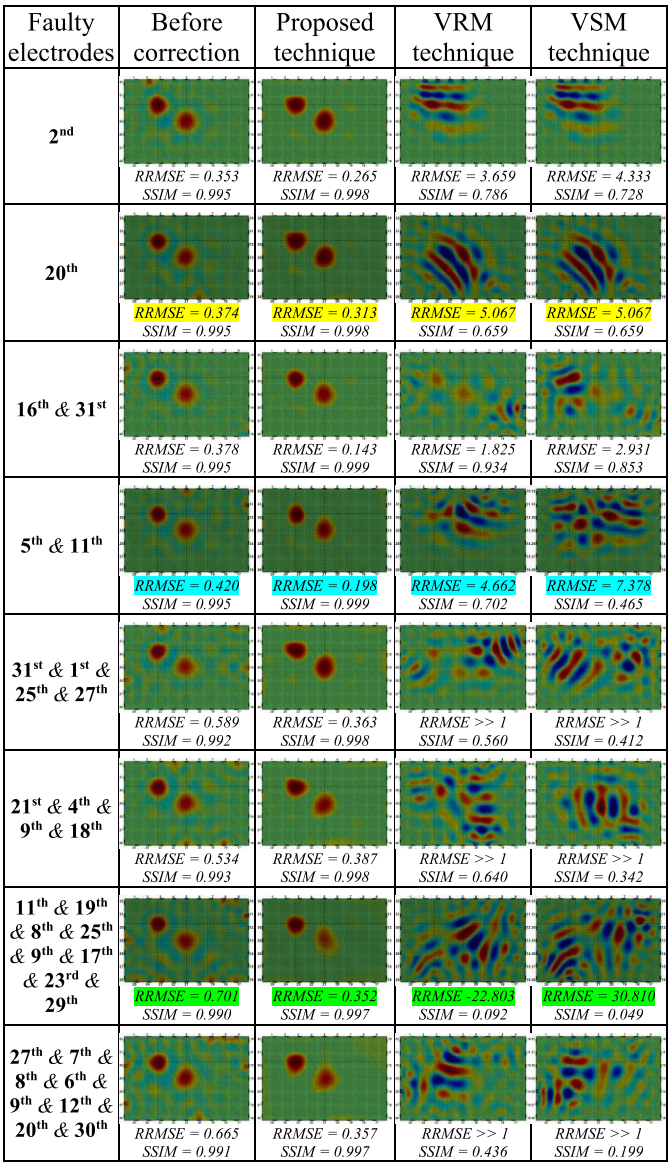

Fig. 16. Verification of the proposed method using the model number 3rd, and electrodes are poor connected.

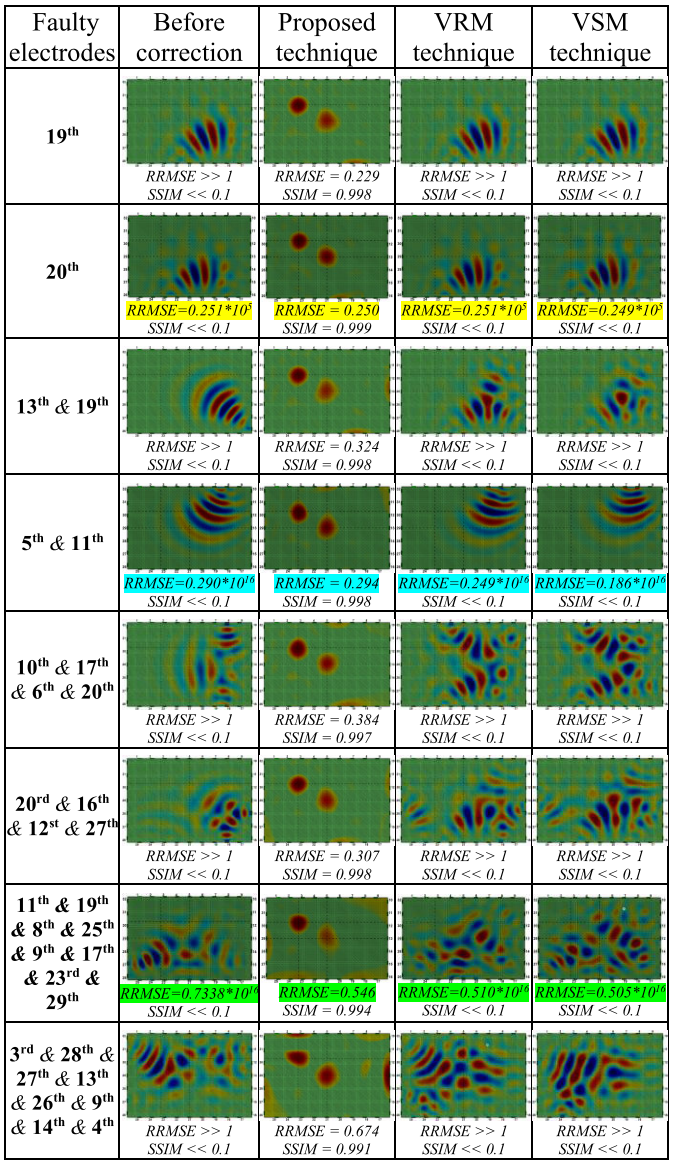

Fig. 17. Verification of the proposed method using the model number 3rd, and electrodes are detached.

locates in the center of the OUT is worse than when the damage locates near the boundary. For example, when two electrodes (the 5th and 11th electrodes) are poorly connected, the RRMSE value is 0238 when damage is located near the specimen boundary and is 0296 when damage is located in the specimen center. When eight electrodes (the 11th, 19th, 8th, 25th, 9th, 17th, 23rd, and 29th electrodes) are detached, the RRMSE value of image with damage in the specimen center is 0873, worse than the RRMSE values when damage near the specimen boundary, which is 0631. However, the SSIM values of model first and second in these cases have only minor differences. The results demonstrate that reconstructed images from data compensated by SURFEIT are similar to the reference image, regardless of the location of damages.

In the last test, the effectiveness of SURFEIT to model damages at different locations is listed as the 3rd test (see Fig. 9). Model 3 contains damages in both center and corner of OUT. The results are shown in Figs. 16 and 17 for the cases when faulty electrodes are poorly connected and detached, respectively. Faulty electrodes in all cases are also selected randomly. The three cases, when one electrode (20th electrode), two electrodes (5th and 11th), and eight electrodes (11th, 19th, 8th, 25th, 9th, 17th, 23rd, and 29th) are faulty, are again tested.

The results show that when faulty electrodes are poorly connected, the proposed techniques can offer reconstructed images with SSIM values in the range 0.997–0.999, while the images without compensation have SSIM values in the range 0.990–0.995. The RRMSE values of images with the proposed compensation range from 0.143 to 0.387. When faulty electrodes are detached, the images with the proposed techniques also have good quality, with SSIM ranges from 0.991 to 0.999 and RRMSE ranges from 0.229 to 0.674.

C. Statistical Evaluation and Optimization

For more detailed evaluation, the relationship between SSIM values and number of faulty electrodes is statistically analyzed.

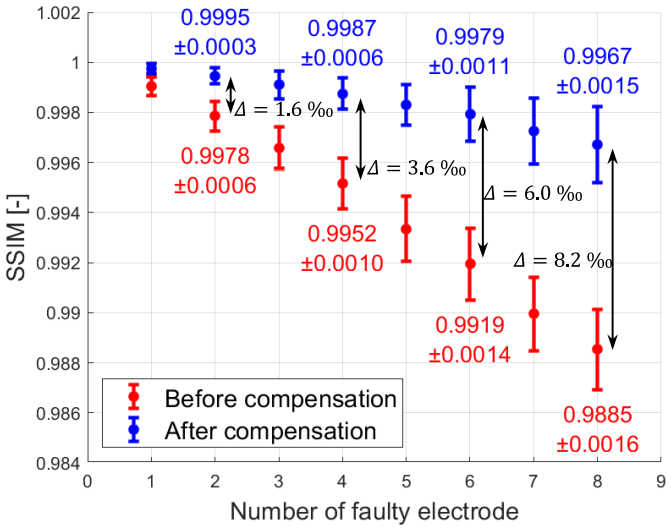

Fig. 18. SSIM values of reconstructed images before and after using the proposed data compensation technique.

The EIT models discussed earlier are simulated with varying numbers of faulty electrodes. For each specified number of faulty electrodes, 50 different groups of faulty electrodes are selected at random. The forward problem is shown using FEM to acquire faulty boundary voltage data. The images are then reconstructed using faulty data without applying compensation technique and with applying the proposed compensation technique. The mean value and deviation of SSIM index are then calculated and shown in Fig. 18. The standard deviation is calculated using (13)

$$\sigma = \sqrt{\frac{\sum\left(\mathrm{SSIM}_i - \overline{\mathrm{SSIM}}\right)^2}{N}} \tag{14}$$

where SSIM_i is the SSIM values of each test case, $\overline{\mathrm{SSIM}}$ is the mean values of SSIM_i, and $N = 50$ is the number of test case.

From Fig. 18, it can be observed that the SSIM values of images before and after compensation decrease with the increase of faulty electrode number. However, the proposed compensation technique offers images with higher SSIM or higher quality. The SUREFIT technique also offers lower standard deviation, in other words, better dispersion. For example, when six electrodes are faulty, the images before compensation have the mean value SSIM of 0.9919 with a standard deviation of 0.0014. The images applied compensation technique in such case have the mean value SSIM of 0.9979 and standard deviation of 0.0011.

The relative change of SSIM index values before and after applying the proposed compensation technique is also calculated and shown in Fig. 18. It is able to conclude that with the higher faulty electrode number, the proposed techniques offer higher relative change in SSIM value. To illustrate, the relative change when model contains four faulty electrodes is about 3.6‰, while the relative change when model contains eight faulty electrodes is about 8.2‰. However, it is important to emphasize that the increase of SSIM relative change will be limited when the number of faulty electrodes is larger than 8, due to the difficulty of correctly detect faulty electrodes and

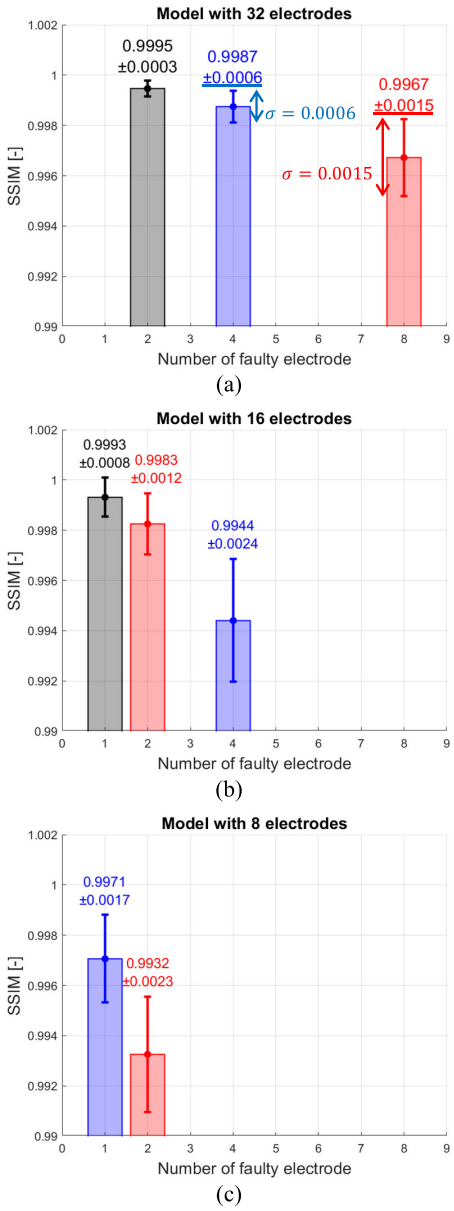

Fig. 19. Verification of the proposed techniques with different numbers of total electrodes and faulty electrodes. (a) Model with 32 electrodes, (b) model with 16 electrodes, and (c) model with eight electrodes.

the significant reduction in the size of used boundary voltage dataset.

The proposed SUFEIT technique is also applied to models similar to the models in Fig. 2 and, however, contains different electrodes. Fig. 19 shows the results of applying proposed techniques to models with different numbers of total electrodes and faulty electrodes. The ratio between faulty electrodes and total electrode is selected as 1/4 (red lines), 1/8 (blue lines), and 1/16 (black lines) for further comparison. The statistical analysis described above is also applied to each model here.

The results show that the quality of image reduces when the number of faulty electrodes increases. For example [Fig. 18(a)], in the case of model with 32 electrodes, the mean SSIM value decreases from 09 987 to 09 867 when the number of faulty electrodes increases from 4 to 8. This is due to the increase of faulty data number, decreasing the size of usable data. However, the SSIM values are always higher

than 0.99, which is near ideal value (the ideal value of SSIM index is 1000).

Also because of the decrease of usable data size, the variation of quality image increases with the increase of faulty electrodes number. As shown in Fig. 19(a), the variation of SSIM index is 00 006 when four electrodes are faulty, about two and half times lower than value of 00 015 when eight electrodes are faulty. The higher variation indicates the larger dispersion or lower reliability of the mean value.

D. Discussion

A new method for fault detection was presented and compared with the existing approaches VSM and VRM used in practice. The existing approaches are based on building a simulation model from measured data for subsequent fault detection. Our SURFEIT approach, unlike the existing approaches where the correction of input data including measurement error is used to create the simulation model, is based on direct modification of the simulation model, which affords reducing the computing time and hardware requirements while also increasing the accuracy of detecting location of the failure in the composite material. This article also details that SURFEIT exhibits disadvantages to existing solutions, which are that our method fails compared to the existing methods when the number of failed electrodes is greater than 1/4 of the total number of electrodes in the data compensation task. In such a case, the existing methods achieve better detection results and better accuracy of determining the location of the fault.

Despite the mentioned drawback, SURFEIT achieves higher quality fault detection accuracy and reliability compared to VRM and VSM methods, which also do not require additional simulation processes to refine the detection. We have therefore compared our new approach with the existing methods in the tasks of detecting the failure of the composite material location and in the task of correcting the location determination if the correct function of the reference measurement point was affected in the impedance measurement process. In such a case, data correction is necessary, and SURFEIT will allow more accurate fault location even in cases of broken electrodes on board the aircraft. Such cases can occur, for example, during aircraft lightning strikes, when we cannot guarantee the correct function of all measured electrodes of the above-mentioned symmetrical arrangement of measuring electrodes. Thus, SURFEIT will make it possible to process cases with nonsymmetrical arrangement and nonsymmetrical distribution of electrodes (measuring points) on the plane, in contrast to the existing methods that use a symmetrical arrangement in principle.

V. Conclusion

This article presents surface fault detection EIT used for fast and efficient detection of the location of the failure of the aircraft composite material used on aircraft. A new method for fault detection was presented and compared with the existing approaches used in practice. In conclusion, it can be stated that SURFEIT shows in the case of 4/16 a ratio of correct detection of 100% compared to the existing approach, where this ratio is around 85%. As shown from the results; in order to achieve maximum accuracy, it is necessary to detect broken electrodes, and thus, we will achieve higher detection reliability. SURFEIT is therefore based on accurate detection of the broken electrode and subsequent correction of the simulation model. This article verified the proposed method and performed tests, for example, in the case of one or two defective electrodes. Also shown were the cases of partially damaged electrodes and the effect on the final determination of the location of the fault on the composite material. Tests have shown that, for example, with a partially damaged electrode, the location reliability is higher than using the approach of isolating a partially damaged electrode with a simulation model creation system. Additional electrode damage tests were analyzed in a system of one, two, four, and eight damaged electrodes out of a total of 32, 16, and 8 measuring electrodes. Similarly, this article analyzed the degrees of damage and their effects on the reliability of the location. Furthermore, the effects of the place of damage to the composite material and the effect on the overall efficiency of determining the location of the fault depending on the damaged electrodes were analyzed. The SURFEIT method shows better results for fault determination and detection compared to the existing methods reported in the current literature.

The verification and evaluation results show that the proposed automatic defective electrode detection technique can achieve very high accuracy when the defective electrodes are up to one quarter of the total number of electrodes. The accuracy of SURFEIT is higher than that achieved by the existing methods as demonstrated from the visual comparisons of the simulated results. The benefit is that additional simulations are not necessary, and thus, the processing load (computing time and hardware requirements) is reduced for fault location with comparable accuracy.

Future work will be combining the proposed method with sensor fusion approaches to increase the performance of EIT-based SHM system. The proposed method also shows that the number of electrodes can be optimized to reduce the total cost and complexity of SHM system, which will be further explored with different arrangements of electrodes.

References

[1] F. C. Campbell, *Structural Composite Materials*. ASM International, 2010.

[2] S. K. Mazumdar, *Composites Manufacturing: Materials, Product, and Process Engineering*. CRC Press, 2001, doi: 10.1201/9781420041989.

[3] K. K. Chawla, *Composite Materials: Science and Engineering*. Cham, Switzerland: Springer, 2019, doi: 10.1007/978-3-030-28983-6.

[4] A. Kelly, R. J. Stearn, and L. N. McCartney, "Composite materials of controlled thermal expansion," *Compos. Sci. Technol.*, vol. 66, no. 2, pp. 154–159, Feb. 2006, doi: 10.1016/j.compscitech.2005.04.025.

[5] A. A. Baker, S. Dutton, and D. Kelly, *Composite Materials for Aircraft Structures* (AIAA Education Series), 2nd ed., Reston, VA, USA: American Institute of Aeronautics & Astronautics, 2004.

[6] B. Wang, S. Zhong, T.-L. Lee, K. S. Fancey, and J. Mi, "Non-destructive testing and evaluation of composite materials/structures: A state-of-the-art review," *Adv. Mech. Eng.*, vol. 12, no. 4, Apr. 2020, Art. no. 168781402091376, doi: 10.1177/1687814020913761.

[7] B. Esp, *Practical Analysis of Aircraft Composites*. Grand Oak Publishing, 2017.

[8] B. Alemour, O. Badran, and M. R. Hassan, "A review of using conductive composite materials in solving lightening strike and ice accumulation problems in aviation," *J. Aerosp. Technol. Manage.*, vol. 11, p. e1919, Mar. 2019, doi: 10.5028/jatm.v11.1022.

[9] S. Imai, E. Blasch, A. Galli, W. Zhu, F. Lee, and C. A. Varela, "Airplane flight safety using error-tolerant data stream processing," *IEEE Aerosp. Electron. Syst. Mag.*, vol. 32, no. 4, pp. 4–17, Apr. 2017, doi: 10.1109/MAES.2017.150242.

[10] S. Paul et al., "Formal verification of safety-critical aerospace systems," *IEEE Aerosp. Electron. Syst. Mag.*, vol. 38, no. 5, pp. 72–88, May 2023, doi: 10.1109/MAES.2023.3238378.

[11] R. Gupta et al., "A review of sensing technologies for non-destructive evaluation of structural composite materials," *J. Compos. Sci.*, vol. 5, no. 12, p. 319, Dec. 2021, doi: 10.3390/jcs5120319.

[12] B. B. Djordjevic, "Nondestructive test technology for the composites," in *Proc. 10th Int. Conf. Slovenian Soc. Non-Destructive*, 2009, pp. 259–265.

[13] M. A. Hamstad, "A review: Acoustic emission, a tool for composite-materials studies," *Experim. Mech.*, vol. 26, no. 1, pp. 7–13, Mar. 1986, doi: 10.1007/bf02319949.

[14] C. Meola, S. Boccardi, G. M. Carlomagno, N. D. Boffa, E. Monaco, and F. Ricci, "Nondestructive evaluation of carbon fibre reinforced composites with infrared thermography and ultrasonics," *Compos. Struct.*, vol. 134, pp. 845–853, Dec. 2015, doi: 10.1016/j.compstruct.2015.08.119.

[15] N. Guo and P. Cawley, "Lamb wave reflection for the quick nondestructive evaluation of large composite laminates," *Mater. Eval.*, vol. 52, no. 3, pp. 404–411, 1994.

[16] F. Kopsaftopoulos and F. K. Chang, "A dynamic data-driven stochastic state-awareness framework for the next generation of bio-inspired fly-by-feel aerospace vehicles," in *Handbook of Dynamic Data Driven Applications Systems*. Springer, 2018, doi: 10.1007/978-3-319-95504-9_31.

[17] R. P. Henderson and J. G. Webster, "An impedance camera for spatially specific measurements of the thorax," *IEEE Trans. Biomed. Eng.*, vol. BME-25, no. 3, pp. 250–254, May 1978, doi: 10.1109/TBME.1978.326329.

[18] H. Hassan and T. N. Tallman, "Precise damage shaping in self-sensing composites using electrical impedance tomography and genetic algorithms," *Struct. Health Monitor.*, vol. 22, no. 1, pp. 372–387, Jan. 2023, doi: 10.1177/14759217221077034.

[19] R. Helena, F. Christophe, F. Nelson, L. Ugo, and J. P. Nunes, "Electrical impedance tomography for damage detection and localization on carbon fibre reinforced polymer composites," in *Proc. 20th Eur. Conf. Compos. Mater., Composites Meet Sustainability*, vol. 3, 2022, pp. 666–673, doi: 10.5075/epfl-298799_978-2-9701614-0-0.

[20] T. Singh and S. Sehgal, "Structural health monitoring of composite materials," *Arch. Comput. Methods Eng.*, vol. 29, no. 4, pp. 1997–2017, Jun. 2022, doi: 10.1007/s11831-021-09666-8.

[21] D. A. M. Amafabia, D. Montalvão, O. David-West, and G. Haritos, "A review of structural health monitoring techniques as applied to composite structures," *SDHM Struct. Durability Health Monitor.*, vol. 11, no. 2, pp. 91–147, 2017, doi: 10.3970/sdhm.2017.011.091.

[22] V. Giurgiutiu, *Structural Health Monitoring of Aerospace Composites*. Academic, 2015, doi: 10.1016/C2012-0-07213-4.

[23] H. Rocha, C. Semprimoschnig, and J. P. Nunes, "Sensors for process and structural health monitoring of aerospace composites: A review," *Eng. Struct.*, vol. 237, Jun. 2021, Art. no. 112231, doi: 10.1016/j.engstruct.2021.112231.

[24] N. Nam Pham, J. Leuchter, and Q. Huy Dong, "FPGA-based measurement instrument for the ERT applications of aerospace composite materials," in *Proc. 20th Int. Conf. Mechatronics*, Dec. 2022, pp. 1–5, doi: 10.1109/ME54704.2022.9983440.

[25] Y. Shi et al., "Compensation of contact impedance variation for cerebral electrical impedance tomography," *IEEE Sensors J.*, vol. 22, no. 24, pp. 24541–24549, Dec. 2022, doi: 10.1109/JSEN.2022.3219586.

[26] C.-L. Hu et al., "Compensation for electrode detachment in electrical impedance tomography with wearable textile electrodes," *Sensors*, vol. 22, no. 24, p. 9575, Dec. 2022, doi: 10.3390/s22249575.

[27] C.-H. Chang et al., "Wireless electrical impedance tomography for pleural effusion analysis," *IEEE Sensors J.*, vol. 23, no. 10, pp. 11025–11033, May 2023, doi: 10.1109/JSEN.2023.3265668.

[28] R. Harikumar, R. Prabu, and S. Raghavan, "Electrical impedance tomography (EIT) and its medical applications: A review," *Int. J. Soft Comput. Eng. (IJSCE)*, vol. 3, no. 4, pp. 193–198, 2013.

[29] J. Wagner, S. Gschoßmann, and M. Schagerl, "On the capability of measuring actual strain values with electrical impedance tomography using planar silkscreen printed elastoresistive sensors," *IEEE Sensors J.*, vol. 21, no. 5, pp. 5798–5808, Mar. 2021, doi: 10.1109/JSEN.2020.3036736.

[30] Y. Shi, K. Yang, M. Wang, Y. Lou, and F. Fu, "Robust compensation of contact impedance change with fully connected neural network in brain EIT," *IEEE Sensors J.*, vol. 23, no. 17, pp. 20169–20179, Sep. 2023, doi: 10.1109/JSEN.2023.3296078.

[31] W. R. B. Lionheart, "EIT reconstruction algorithms: Pitfalls, challenges and recent developments," *Physiological Meas.*, vol. 25, no. 1, pp. 125–142, Feb. 2004, doi: 10.1088/0967-3334/25/1/021.

[32] B. M. Graham and A. Adler, "Objective selection of hyperparameter for EIT," *Physiological Meas.*, vol. 27, no. 5, pp. 65–79, May 2006, doi: 10.1088/0967-3334/27/5/s06.

[33] V. Sarode, S. Patkar, and A. N. Cheeran, "Comparison of 2-D algorithms in ElT based image reconstruction," *Int. J. Comput. Appl.*, vol. 69, no. 8, pp. 6–11, May 2013, doi: 10.5120/11860-7642.

[34] M. Cheney, D. Isaacson, J. C. Newell, S. Simske, and J. Goble, "NOSER: An algorithm for solving the inverse conductivity problem," *Int. J. Imag. Syst. Technol.*, vol. 2, no. 2, pp. 66–75, Jun. 1990, doi: 10.1002/ima.1850020203.

[35] A. Adler and W. R. B. Lionheart, "Uses and abuses of EIDORS: An extensible software base for EIT," *Physiological Meas.*, vol. 27, no. 5, pp. 25–42, May 2006, doi: 10.1088/0967-3334/27/5/s03.

[36] A. E. Hartinger, R. Guardo, A. Adler, and H. Gagnon, "Real-time management of faulty electrodes in electrical impedance tomography," *IEEE Trans. Biomed. Eng.*, vol. 56, no. 2, pp. 369–377, Feb. 2009, doi: 10.1109/TBME.2008.2003103.

[37] G. Zhang et al., "Fast detection and data compensation for electrodes disconnection in long-term monitoring of dynamic brain electrical impedance tomography," *Biomed. Eng. OnLine*, vol. 16, no. 1, pp. 1–23, Dec. 2017, doi: 10.1186/s12938-016-0294-7.

Ngoc Nam Pham received the Ing. (M.Sc.) degree in microelectronics from the Brno University of Technology, Czech Republic, in 2023. He is now studying for a doctorate with the Department of Microelectronics and cooperates, Le Quy Don Technical University, Hanoi, Vietnam.

His main field of scientific activity is the measurement, simulation, and failure analysis of composite materials used in aircraft technology. The goal of his dissertation is the fusion of data in the determination of defects in the structure of a composite material using electrical impedance tomography.

Jan Leuchter received the Ing. (M.Sc.) degree in aviation avionics systems from Military University, Brno, Czech Republic, and the Ph.D. degree in theoretical engineering, in 1998 and 2002, respectively.

He currently works with the Institute of Microelectronics, Brno University of Technology. He also works with the Faculty of Transport, University of Pardubice, Brno. His main area of scientific activity is avionics, measurement, and EMC in aviation. In particular, he specializes in the field of electromagnetic immunity and power sources. Other main areas of research are measurement and power electronics.

Erik Blasch (Fellow, IEEE) is a Principal Scientist with the U.S. Air Force Research Laboratory (AFRL), Information Directorate, Rome, NY, USA. From 2000 to 2009, he was the Information Fusion Evaluation Tech Lead of the AFRL Sensors Directorate—Comprehensive Performance Assessment of Sensor Exploitation (COMPASE) Center, Rome, supporting AF and DARPA evaluations. From 2009 to 2012, he was an Exchange Scientist to Defense Research and Development Canada (DRDC) at Valcartier, Quebec, QC, Canada. He was previously an Adjunct Electrical Engineering Professor at Wright State University, Dayton, OH, USA, teaching signal processing, target tracking, and information fusion from 2000 to 2010, and the Air Force Institute of Technology, Dayton. He is also a Reserve Lt. Col. with the Air Force Office of Scientific Research (AFOSR), Arlington, VA, USA, dc supporting physics, electronics, and nanotechnology developments.

Dr. Blasch is a Fellow of SPIE and an Associate Fellow of AIAA.